Original Article

Sensitivity and specificity of magnetic resonance imaging in routine diagnosis of pulmonary lesions: a comparison with computed tomography

Shuyi Yang[1,2,3,4], Fei Shan[4], Yuxin Shi[4], Tiefu Liu[5], Qingle Wang[1,2,3], Haoling Zhang[1,2,3], Xingwei Zhang[1,2,3], Shan Yang[1,2,3], Zhiyong Zhang[1,2,3,4]

[1]Department of Radiology, Zhongshan Hospital, Fudan University, Shanghai, China; [2]Shanghai Institute of Medical Imaging, Shanghai, China; [3]Department of Medical Imaging, Shanghai Medical College, Fudan University, Shanghai, China; [4]Department of Radiology, Shanghai Public Health Clinical Center, Fudan University, Shanghai, China; [5]Department of Scientific Research, Shanghai Public Health Clinical Center, Fudan University, Shanghai, China

Contributions: (I) Conception and design: Shuyi Yang, F Shan, Y Shi, X Zhang, Shan Yang, Z Zhang; (II) Administrative support: Shuyi Yang, F Shan; (III) Provision of study materials or patients: Q Wang, H Zhang; (IV) Collection and assembly of data: Shuyi Yang, F Shan; (V) Data analysis and interpretation: Shuyi Yang, F Shan, Shan Yang; (VI) Manuscript writing: All authors; (VII) Final approval of manuscript: All authors.

Correspondence to: Zhiyong Zhang, MD. No. 180 Fenglin Road, Xuhui, Shanghai 200032, China; No. 2901 Caolang Road, Jinshan, Shanghai 201508, China. Email: zhyzhang@fudan.edu.cn; Shan Yang, MD. No. 180 Fenglin Road, Xuhui, Shanghai 200032, China. Email: yang.shan@zs-hospital.sh.cn.

Background: State-of-the-art thoracic magnetic resonance imaging (MRI) plays a complementary role in the assessment of pulmonary nodules/masses which potentially indicate to cancer. We aimed to evaluate the sensitivity and specificity of MRI in diagnosis of pulmonary nodules/masses.

Methods: Sixty-eight patients with computed tomography (CT)-detected pulmonary nodules/masses underwent 3T MRI (T1-VIBE, T1-starVIBE, T2-fBLADE turbo spin-echo, and T2-SPACE). The detection rate was calculated for each of the different subgroups of pulmonary nodules according to lung imaging reporting and data system (Lung-RADS). The four MRI sequences were compared in terms of detection rate and image quality-signal to noise ratio (SNR), contrast to noise ratio (CNR) and 5-point scoring scale. Agreement of lesion size measurement between CT and MRI was assessed by intraclass correlation coefficient (ICC). The picture-SNR, lesion-SNR and CNR of each sequence were analyzed by Mann-Whitney U test.

Results: In total, 232 pulmonary lesions were detected by CT. The CT showed 86 solid nodules (SNs) <6 mm, 15 SNs between 6–8 mm, 35 SNs between 8–15 mm, and 52 SNs between 15–30 mm. The T1-VIBE, T1-starVIBE, T2-fBLADE TSE and T2-SPACE sequences accurately detected 141 SNs (141/188, 75%/83.3%), 150 SNs (150/188, 79.8%/100%), 166 SNs (166/188, 88.3%/66.7%) and 169 SNs (169/188, 89.9%/53.3%), respectively. Four ground glass nodules (GGNs) (4/6) were detected by T2-fBLADE TSE. Twelve part-solid nodules (PSNs) (12/22) were detected by T1-VIBE and 20 PSNs (20/22) by T2-SPACE. A total of 100 lesions (2.2±1.4 cm, 0.8–7.3 cm) were accurately detected and measured by the four MRI sequences with ICC >0.96. The picture-SNR, lesion-SNR and CNR by T1-starVIBE were higher than those by T1-VIBE (P<0.001). The lesion-SNR and CNR by T2-fBLADE TSE were higher than those by T2-SPACE (P=0.006, 0.038). 86% of images by T1-starVIBE, 92% by T2-fBLADE TSE, 90% by T2-SPACE and 93% by T1-VIBE were scored 3 or more.

Conclusions: MRI achieves high sensitivity and specificity for different type of pulmonary nodules detection and is an effective alternative to CT as a diagnostic tool for pulmonary nodules.

Keywords: Pulmonary nodule; magnetic resonance imaging (MRI); lung imaging reporting and data system (Lung-RADS); computed tomography (CT)

Submitted Mar 21, 2022. Accepted for publication Aug 26, 2022.
doi: 10.21037/jtd-22-370
View this article at: https://dx.doi.org/10.21037/jtd-22-370

Introduction

Lung cancer is a leading cause of cancer-related mortality worldwide, accounting for nearly 1.8 million deaths in 2020 (1). Diagnosis and management at early stage is vital to increase survival rate of lung cancer. Low dose computed tomography (LDCT) is a common technique for lung cancer screening, which has reduced lung cancer-related mortality by 20% (2). Results of the Dutch-Belgian Randomized Lung Cancer Screening (NELSON) Trial showed that lung-cancer mortality was significantly decreased among those who underwent volume computed tomography (CT) screening (3). However, repetitive use of CT with ionizing radiation effect has carcinogenic risk, particularly in patients who require reviews over a prolonged period (4,5). Therefore, magnetic resonance imaging (MRI) as the radiation-free lung imaging technique has recently attracted more and more attentions.

Since the clinical introduction of MRI, the chest scan has been one of its most challenging applications mainly due to the low proton density and extremely rapid T2* decay of the lung, susceptibility artifacts at air-tissue interfaces, and physiological motions including respiration and cardiac pulsation of the thorax (6,7). However, MRI retains advantages in terms of soft-tissue contrast and the ability for functional and cine-based imaging (8). With the advancement of MRI techniques, state-of-the-art thoracic MRI plays a complementary role in the management of patients with various chest diseases and especially in the detection and evaluation of pulmonary nodules or masses which potentially indicate to cancer (9).

Two major MRI sequences widely used in pulmonary nodules detection are the turbo spin-echo (SE)-based and the gradient-echo (GRE)-based techniques, with varying results for reduction of cardiac- and respiratory-motion artifacts (9). Currently, a respiratory-navigated sequence by radial k-space acquisition, commonly known as PROPELLER (GE, Milwaukee, WI, USA), fBLADE (Siemens, Erlangen, Germany), or MultiVane (Philips, Best, the Netherlands), provides excellent T2 contrast because of its insensitive to cardiac motion, and becomes a preferred alternative for mitigating respiratory motion (8,10-12). Although the pulmonary lesion detection by 3D T1-weighted gradient echo volumetric interpolated breath-hold examination (VIBE) sequence is less sensitivity than that by TSE imaging (9), the VIBE sequence with radial acquisition trajectory by stack-of star (starVIBE) is insensitive to motion and magnetic susceptibility artifacts, therefore, it can improve the image quality (11,13).

For fat-suppressed T2-weighted imaging, short tau inversion recovery (STIR) sequences provide extreme T2-weighting. In addition, the nodule detection capability of STIR is deemed to be equal to or even better than that of other contrast techniques (9,14,15). A close variant of chemical fat suppression is spectral inversion recovery (known as SPAIR for Siemens or ASPIR for GE), which also satisfies for detection of pulmonary nodules (8,14).

Sampling perfection with application optimized contrasts using different flip angle evolution (SPACE) is another 3T MRI sequence that can achieve thin-slice imaging. We assume that the thin-slice can provide higher detection sensitivity and more pulmonary nodule characteristics, which is rarely used in routine pulmonary MRI. Therefore, the present study aimed to evaluate the sensitivity, specificity, and image quality of 3T MRI sequences in detection of pulmonary nodule and compare them with CT findings, so as to provide an ideal MRI protocol for detection of pulmonary nodules in the routine clinical practice. We present the following article in accordance with the STARD reporting checklist (available at https://jtd.amegroups.com/article/view/10.21037/jtd-22-370/rc).

Methods

Patients

From October 2018 to October 2019, 156 patients with pulmonary nodules or masses detected by CT were advised to undergo dedicated thoracic MRI according to a protocol approved by the Institutional Review Board of Shanghai Public Health Clinical Center (No. 2019-S021-02). Written informed consent was obtained from all patients before MRI scans. The study was conducted in accordance with the Declaration of Helsinki (as revised in 2013). The inclusion criteria were as follows: (I) pulmonary nodules or masses clearly depicted by CT with the slice thickness/interval of 1 mm/1 mm; (II) pulmonary nodules or masses underwent MRI scan by sequences of T1-VIBE, T1-starVIBE, T2-fBLADE TSE and T2-SPACE. The exclusion criteria were as follows: (I) patients with contraindication for MR imaging, including pacemaker, ferromagnetic implants, and claustrophobia; (II) patients with severely impaired pulmonary function, such as acute exacerbated chronic obstructive pulmonary disease and interstitial pneumonia; (III) patients with lower breath-hold capability and compliance, and larger motion artifact. Finally, sixty-eight

Table 1 Imaging parameters of the MRI scan protocol

Parameter	T1-VIBE	T1-starVIBE	T2-fBLADE	T2-SPACE
TR (ms)/TE (ms)	3.67/1.78	2.79/1.39	3,740.0/69.0	1,600.0/108.0
Flip angle (°)	5	5	130	–
FOV	380	380	380	380
Matrix	320	320	320	320
Slice thickness (mm)	3.0	3.0	3.0	3.0
Slice interval (mm)	0.6	0.6	0.6	0
Voxel (mm^3)	1.2×1.2×3.0	1.2×1.2×3.0	1.2×1.2×3.0	1.2×1.2×3.0
Gating	None	None	Respiratory-trigger	Respiratory-trigger
Breath-hold	Yes	No	No	No
Fat-suppression	SPAIR	SPAIR	STIR	SPAIR
No. of average	2	1	–	2
Acquisition plane	Axial	Axial	Axial	Axial
Scanning time (s)	22	103	131	323

MRI, magnetic resonance imaging; TR, repetition time; TE, echo time; FOV, field of view.

patients including 47 males and 21 females with median age of 59 years (17–78 years) were enrolled in this study. MRI and CT were performed with a maximum of 12 days interval between the two examinations (median interval 3 days).

CT

For acquisition, the patients lay in the supine position on a 320-detector CT (Aquilion Vision, Canon Medical Systems, Japan) in full inspiration. Scanning range was from the level of the thoracic inlet to the inferior level of the costophrenic angle. The CT protocol included the following parameters: detector width, 80×0.5 mm; pitch, 0.813; tube voltage, 120 kV; automatic tube current with SD 10 (Sure Exp 3D set, maximum: 440 mA, minimum: 60 mA); The radiation dose of the thoracic CT was calculated in terms of the dose-length product (DLP). Average radiation dose was 5.2±0.7 mSv. All CT images with the slice thickness/interval of 1 mm/1 mm were reconstructed by means of adaptive iterative dose-reduction with three-dimensional processing (AIDR 3D, standard) and a high frequency reconstruction algorithm (FC56) for the lung window setting, and with a standard reconstruction algorithm (FC17) for the mediastinum window setting. The width and level of the lung window were adjusted appropriately by the reference standards of 1,600 and –600 Hounsfield unit (Hu).

MRI

All patients underwent 3T MRI (MAGNETOM Skyra, Siemens Healthcare, Erlangen, Germany) with a 32-channel body-phased array coil. The patients were instructed to lie in supine position, with their arms raising above their body, and to breathe freely. The pulmonary lesions were positioned in the positioning map of horizontal, sagittal and coronal position. The lesions were regarded as the center of the map to determine the number of scan layers along the long axis of the body so that the lesions and adjacent pulmonary parenchyma were covered. The parameters of MRI sequences were summarized in *Table 1*, including breath-hold T1-VIBE (SPAIR), free-breathing T1-star VIBE (SPAIR), respiratory triggered (RT) T2-fBLADE TSE (STIR), and RT-T2-SPACE (SPAIR). The total scan time was nearly 10 minutes due to the respiratory status of patients.

Image analysis

All images were reviewed and analyzed anonymously by picture archiving and communication systems (PACS) and RadiAnt DICOM Viewer 4.6.9 (Medixant, Poznan, Poland, https://www.radiantviewer.com/).

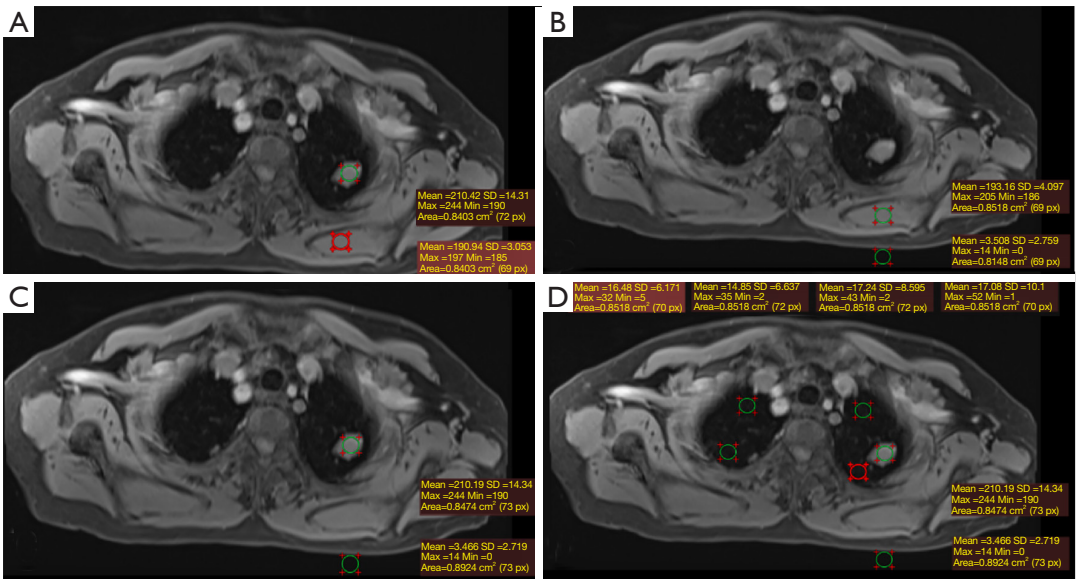

Figure 1 A 41-year-old male with 1.6 cm SN in the left upper lobe. The diagram of lesions' LMR, picture-SNR, lesion-SNR and lesion-CNR; T1-starVIBE. (A) LMR = SI_{lesion}/SI_{muscle} =210.42/190.94≈1.10; (B) picture-SNR = SI_{lesion}/noise =193.16/2.759≈70.01; (C) lesion-SNR = SI_{lesion}/noise = 210.19/2.719≈77.30; (D) lesion-CNR = [SI_{lesion} – mean(SI_{lung})]/noise = [210.19–(16.48+14.85+17.24+17.08)/4]/2.719≈71.27. SN, solid nodule; LMR, lesion to muscle ratio; SNR, signal to noise ratio; CNR, contrast to noise ratio; SI, signal intensity.

CT image analysis

A radiologist with 30 years of experience (Y.S) evaluated the pulmonary lesions detected by CT in routine clinical practice. The location, size, and type of each pulmonary lesions were recorded. Lesion size was defined as the mean values of the longest and shortest axial diameters. The nodules were classified into ground glass nodules (GGNs), part-solid nodules (PSNs), and solid nodules (SNs) according to the attenuation on CT according to the Fleischner Society Guidelines (16,17). The nodules were categorized into 4 groups based on size according to the lung imaging reporting and data system (Lung-RADS) (16,17): <6, 6–8, 8–15, or >15 mm in diameter. The largest level of each lesion was selected for measurement. As CT was considered as the gold standard for nodule detection, a nodule detected by MRI but not by CT was defined as false positive, a nodule diagnosed by CT but not by MRI was defined as a false negative. Sensitivity was defined by true positive result/true positive result + false negative results, while specificity was defined by true negative result/true negative result + false positive results.

MRI image analysis

The MRI data analysis was blindly performed by two radiologists with 20 years (F.S, observer 1) and 6 years (Shuyi Yang, observer 2) of experience in chest imaging diagnosis, respectively. To eliminate detection bias, both of these observers were unaware of the CT findings. Each MRI sequences were evaluated independently by both readers in a blinded fashion in the interval time of 4 weeks. The size and location of each lesion in MR imaging were recorded.

Mean signal intensity of the pulmonary lesions (SI_{lesion}) were measured by focusing the regions of interest (ROIs) on lesions larger than 0.8cm in diameter. The ROIs included the entire scope of the lesions and avoided visible necrosis components (liquefaction necrosis signal intensity), large vessels, and other non-signal areas. The same pixel (error is less than 5%) of ROI was also drawn in the dorsal muscle at the same slice to achieve the mean muscles' signal intensity (SI_{muscle}). The lesion to muscle ratio (LMR) was then calculated by the equation: LMR = SI_{lesion}/SI_{muscle} (low ≤0.75, moderate >0.75 & ≤1.5, high >1.5) (*Figure 1A*). The picture signal to noise ratio (picture-SNR), lesion-SNR and contrast to noise ratio (CNR) were calculated to compare the image quality and the ability of those 4 MRI sequences in assessing signal intensity of pulmonary lesions. Picture-SNR was calculated by mean SI_{muscle}/noise. Lesion-SNR by

mean SI_{lesion}/noise, and CNR by (mean SI_{lesion} – mean SI_{lung})/noise (*Figure 1B-1D*).

Two radiologists also independently evaluated T1-VIBE, T1-starVIBE, T2-fBLADE TSE and T2-SPACE images in terms of visualization of normal structures, degree of noise and artifacts, and overall acceptability. The 5-point scale was used as follows (18): 1 point, unacceptable (with heavy noise/artifacts, the lesions can't be detected, invisible peripheral pulmonary structures, indistinguishable lobar bronchial walls); 2 points, suboptimal (with above-average noise/artifacts, the lesions can be detected with unclear margin, barely visible peripheral pulmonary structure, visible lobar bronchial walls); 3 points, satisfactory (with average/acceptable noise/artifacts, the lesion can be detected with integrate margin, small lesions may be misdiagnosed, visible peripheral pulmonary structure, visible segmental bronchial walls); 4 points, above average (with less than average noise/artifacts, the lesions can be depicted clearly, the small lesions can be detected, visible peripheral pulmonary structure, visible sub-subsegmental bronchial walls); 5 points, excellent (with minimal artifacts/noise, lesions can be depicted clearly, visible peripheral pulmonary structure, visible sub-subsegmental bronchial walls). The final score of each sequence was determined by consensus of the two readers. Acceptability of each set of images was defined as the final score of 3 or more. Four reading sessions were provided with 4-week interval to avoid consecutive reading of four sequences of the same patients.

Statistical analysis

Statistical analysis was conducted using IBM SPSS 26 (IBM Corporation, Armonk, New York, USA, https://www.ibm.com/analytics/spss-statistics-software) and MedCalc 18.11.3 (MedCalc Software Bvba, Ostend, Belgium, https://www.medcalc.org/). All continuous variables were presented as "mean ± standard deviation", while categorical variables were shown as percentage. The intraclass correlation coefficient (ICC) was used to assess the consistence of lesion diameter measurements between CT and MRI sequences. As the ICC approached 1, the diameter measurement consistency between the tested methods was better (excellent: >0.75, mild: 0.40< ICC ≤0.74, poor: ≤0.40). The picture-SNR, lesion-SNR, and CNR of each sequence were compared by Mann-Whitney U test. All test was two-tailed, $P<0.05$ was considered statistically significant.

Results

Pulmonary lesions detection rate by MRI

The CT imaging displayed 232 pulmonary lesions in 68 patients, comprising 188 SNs (1.0±0.8 cm, range, 0.3–3.0 cm), 22 PSNs (average 0.8 cm, range, 0.4–2.4 cm), 6 GGNs (average 0.7 cm, range, 0.4–0.9 cm), 1 ground glass mass (GGM), and 15 solid masses. According to the Lung-RADS (16,17), of the 188 SNs, the diameters of 86 nodules were <6 mm, 15 nodules between 6 and 8 mm, 35 nodules between 8 and 15 mm, and 52 nodules between 15 and 30 mm. The T1-VIBE, T1-starVIBE, T2-fBLADE TSE, and T2-SPACE sequences accurately detected 141 SNs, 150 SNs, 166 SNs and 169 SNs, respectively (*Figure 2*). The detection rate of pulmonary SNs by MRI were showed in *Table 2*. One GGN (1/6, 16.7%) was detected by T1-starVIBE, 4 GGNs (4/6, 66.7%) by T2-fBLADE TSE, and 2 GGNs (2/6, 33.3%) by T2-SPACE, no GGN was detected by T1-VIBE. Twelve PSNs (12/22, 54.6%) were detected by T1-VIBE, 15 PSNs (15/22, 68.2%) by T1-starVIBE, 18 PSNs (18/22, 81.8%) by T2-fBLADE TSE, and 20 PSNs (20/22, 90.9%) by T2-SPACE (*Figure 3*). The GGM was detected by T2-fBLADE TSE and T2-SPACE, but not by T1WI (*Figure 4*).

Pulmonary lesions depiction and image quality evaluation

CT detected 111 pulmonary nodules or mass larger than 0.8 cm in diameter, from which 11 lesions (4 SNs in diameter of 8–10 mm, 5 GGNs, and 2 lesions with calcification) were excluded due to undetectable by all 4 MRI sequences. Finally, a total of 100 lesions (2.2±1.4 cm, 0.8–7.3 cm) were detected by T1-VIBE, T1-starVIBE, T2-fBLADE TSE, and T2-SPACE at the same time. The lesion size measured by MRI sequences was excellently consistent with that by CT with ICC value bigger than 0.96 (*Table 3*).

LMR was measured to depict signal characteristics of the pulmonary lesions. The LMRs were 1.2±0.3, 1.0±0.2, 2.6±1.4 and 2.2±0.8 in T1-VIBE, T1-starVIBE, T2-fBLADE, and T2-SPACE, respectively. Eighty-one lesions (81%) were with high LMR by T2-weighted imaging (T2WI), while eleven (11%) lesions and none lesion with high LMR by T1-VIBE and T1-starVIBE (Table S1). For T1WI sequences, 80 (80%) lesions and 89 (89%) lesions with moderate LMR by T1-VIBE and T1-starVIBE. The picture-SNR, lesion-SNR and CNR by T1-starVIBE were 245.8±56.2, 248.7±73.4, and 211.3±66.2, respectively, all

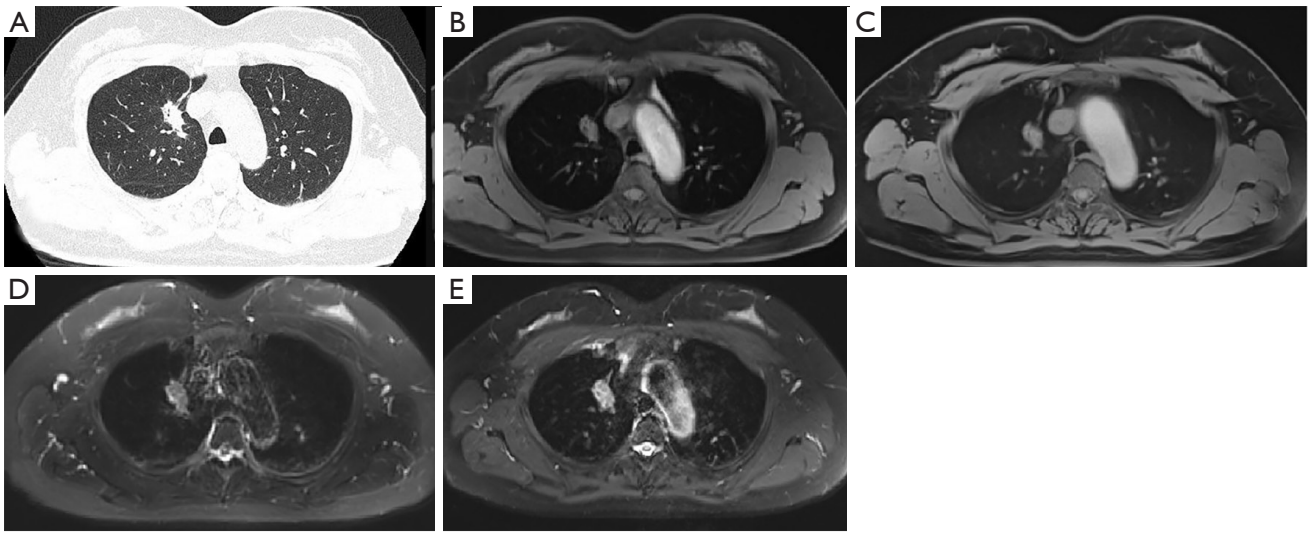

Figure 2 A 53-year-old female with 1.95 cm SN in the right upper lobe. The nodule was well depicted on the CT axial (A), T1-VIBE (B), T1-starVIBE (C), T2-fBLADE (D) and T2-SPACE (E). The nodule showed moderate LMR in T1-VIBE and T1-starVIBE, while high LMR in T2-fBLADE and T2-SPACE. SN, solid nodule; CT, computed tomography; LMR, lesion to muscle ratio.

Table 2 Detection rate/sensitivity and specificity of MRI according to Lung-RADS in SNs

Imaging methods	<6 mm (mount/percentage)	≥6, <8 mm (mount/percentage)	≥8, <15 mm (mount/percentage)	≥15, ≤30 mm (mount/percentage)	Total (mount/sensitivity)	Specificity
CT	86/100	15/100	35/100	52/100	188/100%	–
T1WI-VIBE	45/52.3	12/80	32/91.4	52/100	141/75%	83.3%
T1WI-starVIBE	53/61.6	13/86.7	32/91.4	52/100	150/79.8%	100%
T2WI-fBLADE	66/76.7	14/93.3	34/97.1	52/100	166/88.3%	66.7%
T2WI-SPACE	68/79.1	14/93.3	35/100	52/100	169/89.9%	53.3%

MRI, magnetic resonance imaging; Lung-RADS, lung imaging reporting and data system; SN, solid nodule; CT, computed tomography.

of which were higher than those by T1-VIBE (157.4±68.0, 192.3±95.0, 183.5±92.5, respectively, P<0.001). The lesion-SNR and CNR by T2-fBLADE were 253.9±130.1 and 235.4±131.9, both of which were higher than those by T2-SPACE (208.5±120.8, P=0.006; 198.0±113.4, P=0.038, respectively). The picture-SNR was 99.4±30.8 by T2-fBLADE and 99.0±54.1 by T2-SPACE; however, the difference was not statistically significant (P=0.613). For images with final score ≥3, 93% of images by T1-VIBE, 86% by T1-starVIBE, 92% by T2-fBLADE, and 90% by T2-SPACE were considered sufficient for clinical diagnosis. No sequences got score of 1 and no sequence of T2WI achieved score 5 (*Table 4*).

Discussion

Our study investigated the detection capability of pulmonary nodules by clinical routine MRI sequences and achieved acceptable results. Our results confirmed prior reports that the T2WI sequence was more effective in detecting pulmonary nodules than T1WI (9,19-22).

According to Lung-RADS, only nodules ≥6 mm have a slightly elevated risk (≥1%) of malignancy and require short-term follow-up or further investigation (16,17). In our study, for SN <6 mm (Lung-RADS score 2), T1-VIBE had the lowest detection sensitivity (52.3%), while T2WI had higher sensitivity (76.7% by T2-fBLADE, 79.1% by T2-SPACE). Yet, the misdiagnosed nodules were with

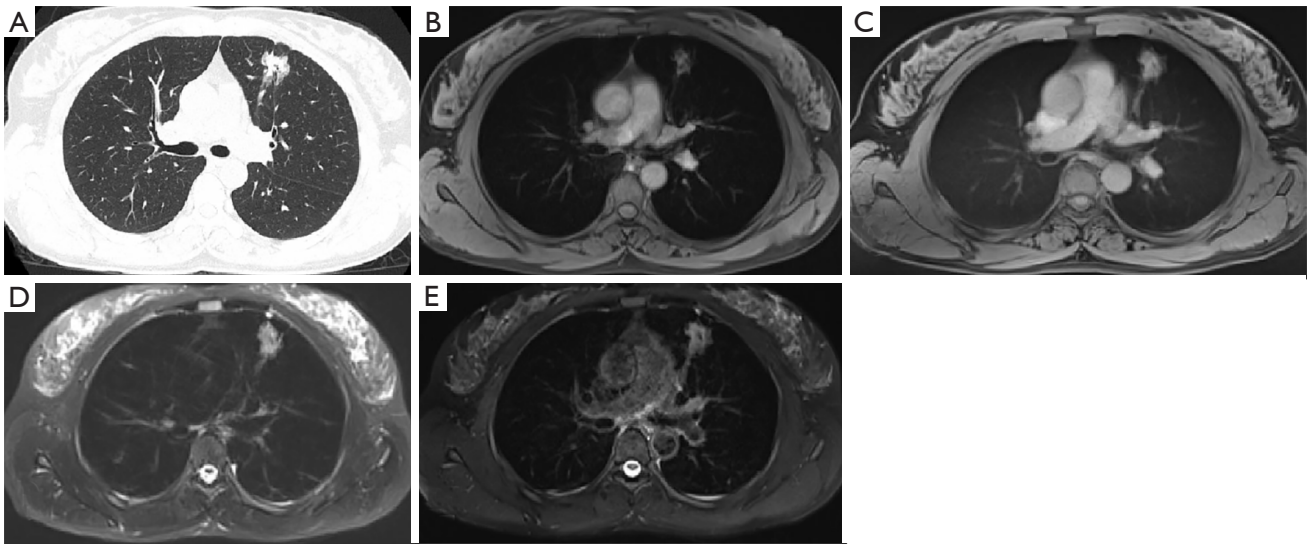

Figure 3 A 46-year-old female with 2.34 cm PSN in the left upper lobe. The nodule was well depicted on the CT (A), T1-VIBE (B), T1-starVIBE (C), T2-fBLADE (D) and T2-SPACE (E). The nodule showed low and moderate LMR in T1-VIBE and T1-starVIBE, while high LMR in T2-fBLADE and T2-SPACE. PSN, part-solid nodule; CT, computed tomography; LMR, lesion to muscle ratio.

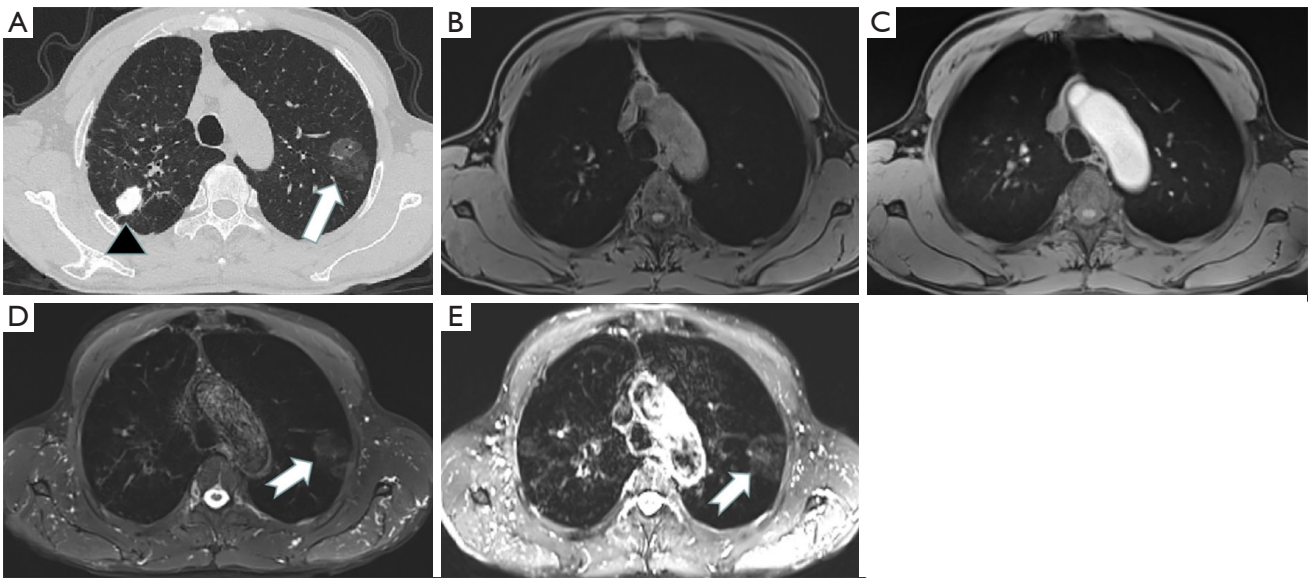

Figure 4 A 67-year-old male with 3.27 cm GGM in the left upper lobe. The GGM was well depicted on the CT (A, "arrow"), T2-fBLADE (D, "swallow tail arrow") and T2-SPACE (E, "swallow tail arrow"), but cannot be depicted by T1-VIBE (B) and T1-starVIBE (C). The nodule showed low LMR in T2-fBLADE and T2-SPACE. Calcified nodule was well depicted on the CT (A, "triangle"), but cannot be detected by MRI sequences. GGM, ground glass mass; CT, computed tomography; LMR, lesion to muscle ratio; MRI, magnetic resonance imaging.

Table 3 The consistence analysis of lesions size measurement compared to CT

Imaging methods	Size (cm), mean ± SD, range	ICC	95% CI
CT	2.21±1.36, 0.8–7.26	–	–
T1WI-VIBE	2.05±1.33, 0.7–7.2	0.9825	0.9741–0.9882
T1WI-starVIBE	2.16±1.37, 0.6–7.065	0.9742	0.9619–0.9826
T2WI-fBLADE	2.25±1.41, 0.8–7.695	0.9630	0.9455–0.9750
T2WI-SPACE	2.18±1.39, 0.7–7.6	0.9737	0.9612–0.9822

CT, computed tomography; SD, standard deviation; ICC, intraclass correlation coefficient; CI, confidence Interval.

Table 4 The final score for each MRI sequence (total number =100)

Score	T1-VIBE, (n/%)	T1-starVIBE, (n/%)	T2-SPACE, (n/%)	T2-fBLADE, (n/%)
1-point	0/0	0/0	0/0	0/0
2-point	7/7	14/14	10 /10	8/8
3-point	45/45	40/40	65/65	53/53
4-point	43/43	41/41	25/25	39/39
5-point	5/5	5/5	0/0	0/0

MRI, magnetic resonance imaging.

lower risk of malignancy. For SNs between 6 and 8 mm with malignant risk of 1–2%, (Lung-RADS score 3), T1-VIBE showed the lowest sensitivity of 80% and T2WI achieved higher sensitivity of 93.3%, which was superior to the published studies showing sensitivity of 75% for 6–8 mm nodules by T1WI (23). Recently, ultra short echo time (UTE), which is used in conjunction with the PD-weighted 3D GRE sequence, has been reported more promising and useful in pulmonary diseases assessment (9,18,24). UTE achieved the sensitivity of 83–94.4% for 6–8 mm nodules (15,25), which was comparable to our results. For SNs between 8 and 15 mm with malignant risk of 5–15% (Lung-RADS score 4A), T1WI reached the sensitivity of 91.4%, T2-fBLADE TSE of 97.1%, and T2-SPACE of 100%. For SNs ≥15 mm with malignant risk of ≥15% (Lung-RADS score 4B), all nodules were detected by MRI. Overall, in our study, T1-starVIBE/T2-fBLADE TSE achieved better performance for SN detection with sensitivity and specificity of 79.8%/88.3% and 100%/66.7%, respectively. Nodules with ground glass appearance on CT are named PSN (with solid component) and GGN (without solid component), which can develop into microinvasive adenocarcinoma or invasive adenocarcinoma. In our study, T2WI is more sensitive for the detection of PSN and GGN. For PSN, T2-fBLADE TSE and T2-SPACE showed the detection sensitivity of 81.8% and 90.9%, while T1-VIBE and T1-starVIBE showed 54.6% and 68.2%. T2-fBLADE TSE and T2-SPACE had the GGN detection sensitivity of 66.7% and 33.3%, while T1-VIBE could not detect GGN. The detection sensitivity of PSN and GGN by MRI was lower than that by UTE reported in previous study (25), yet the number of PSNs and GGNs was too small to analyze nodule detection capability in our study.

Nodule size has also been considered as an effective biomarker for nodule management to reduce lung cancer-specific mortality according to Lung-RADS (16,17). Accurate size measurement contributes to assessment of nodule score and follow-up surveillance. In our study, lesion size measured by MRI sequences produced excellent inter-method consistency with CT. The mean size of lesions measured by T1-VIBE, T1-starVIBE, and T2-SPACE were slightly smaller than that by CT, which was consistent with the reported studies (26,27); this could be explained by that the images acquired by CT were in the state of breath-hold after inspiration, while all the images by T1-starVIBE and T2-fBLADE sequences were acquired in the free-breathing state, resulting in a certain degree of deformation of the lesions (26). The difference of slice thickness and interval between MRI and CT may also affect the consistency of

lesions size measurement. But the very small difference in size between MRI and LDCT is acceptable in routine clinical practice. To depict the signal intensity of lesions, we calculated their LMR. The results showed that most lesions had moderate signal intensity in T1WI and high signal intensity in T2WI. Previous study showed that the signal intensity of lesions might be an indicator of malignant change; however, it was limited by the significant overlapping of their relaxation time (9,28).

Our results demonstrated that MRI was suitable for detection and evaluation of pulmonary nodules. The latest advances of pulmonary MRI technology, such as radial k-space sampling and UTE, have made MRI a potential radiation-free alternative to CT (8,9,11,15,18,20,25-27). The T2-TSE sequence in our study using fast-BLADE (fBLADE) technology, which is periodically rotating overlapping parallel lines radially filling k-space based on non-Cartesian coordinates, can eliminate distorted data, reduce artifacts, and is insensitive to motion and susceptibility artifacts, thereby significantly improving image quality (12). The T2-SPACE sequence is a fast spin-echo three-dimensional imaging, which is characterized by high resolution and high SNR and can achieve thin-slice reconstruction (29). We firstly applied this sequence to pulmonary lesion detection and showed it can improve the detection sensitivity of small pulmonary nodules. Furthermore, we demonstrated that both lesion-SNR and CNR by T2-fBLADE TSE were statistically higher than those by T2-SPACE. However, the difference of picture-SNR by T2-fBLADE TSE and T2-SPACE was not statistically significant. Free-breathing T1-starVIBE using radial k-space data sampling substantially reduced motion-related artifacts, which improve image quality by compensating artifacts from breathing, heart pulsation, and other motions (27,30,31). Our result showed that picture-SNR, lesion-SNR and lesion-CNR by T1-starVIBE were higher than those by T1-VIBE. The previous study also reported that T1-starVIBE was better than T1-VIBE in displaying the morphological characteristics of peripheral solid pulmonary masses, the T1-VIBE was suitable for patients who couldn't comply with breath-hold requirements (11,30). However, the percentage of images with the score of 3 or more by T1-starVIBE was the lowest (86%), suggesting that the T1-VIBE (93%) could achieve better images if the patients had excellent coordination ability, similar to previous reported results (11). The T2-SPACE sequence image had more noise artifacts, and the score ≥3 points ratio (90%) was slightly lower than that of T2-fBLADE (92%).

In summary, the current study suggested a fast and simple scan protocol for routine detection of pulmonary nodules. We recommend T1-VIBE for patients who are able to do breath-holding, while T1-starVIBE, which achieve better image quality than T1-VIBE, for patients who are unable to do breath-holding. T2-fBLADE TSE sequence is optimal for pulmonary nodule evaluation due to its better image quality than T2-SPACE, whereas, T2-SPACE for small nodules due to its high sensitivity despite of its lower specificity.

This study had some limitations. Firstly, the studied images were from a single institution, and nodule numbers were not large enough, especially for GGN and PSN. Multiple institutional research needs to be conducted in future, especially focusing on the GGN and PSN detection by MRI sequences. Secondly, the pathological results of pulmonary nodules were not collected, because the main goal of our study was to investigate the nodule detection rather than nodule evaluation by MRI sequences. Thirdly, UTE was not studied, although it was valuable for nodule detection and depiction in previous studies, it is not a common technique in clinical practice due to its special procedure.

Conclusions

We have demonstrated that MRI, especially the T1-starVIBE and T2-fBLADE, was a more effective strategy for pulmonary nodule detection in comparison with CT, in terms of sensitivity and specificity, making it a useful technique in routine clinical practice.

Acknowledgments

We would like to thank Tiefu Liu for his help in polishing our paper.

Funding: This work was supported by the Shanghai Municipal Science and Technology Commission (No. 18411967100), Shanghai Hospital Development Center (No. SHDC2020CR3080B), National Natural Science Foundation of China (No. 82172030), Shanghai Municipal Science and Technology Commission (No. 22YF1443500) and Ningbo Medical Science and Technology Project (No. 2018A14).

Footnote

Reporting Checklist: The authors have completed the STARD

reporting checklist. Available at https://jtd.amegroups.com/article/view/10.21037/jtd-22-370/rc

Data Sharing Statement: Available at https://jtd.amegroups.com/article/view/10.21037/jtd-22-370/dss

Peer Review File: Available at https://jtd.amegroups.com/article/view/10.21037/jtd-22-370/prf

Conflicts of Interest: All authors have completed the ICMJE uniform disclosure form (available at https://jtd.amegroups.com/article/view/10.21037/jtd-22-370/coif). The authors have no conflicts of interest to declare.

Ethical Statement: The authors are accountable for all aspects of the work in ensuring that questions related to the accuracy or integrity of any part of the work are appropriately investigated and resolved. The study was conducted in accordance with the Declaration of Helsinki (as revised in 2013). The study was approved by Institutional Review Board of Shanghai Public Health Clinical Center (No. 2019-S021-02) and informed consent was taken from all the patients.

References

1. CANCER TODAY Data visualization tools for exploring the global cancer burden in 2020 International Agency for Research on Cancer. Available online: https://gco.iarc.fr/today/home (accessed August 6, 2021).
2. Aberle DR, Adams AM, Berg CD, et al. Reduced lung-cancer mortality with low-dose computed tomographic screening. N Engl J Med 2011;365:395-409.
3. de Koning HJ, van der Aalst CM, de Jong PA, et al. Reduced Lung-Cancer Mortality with Volume CT Screening in a Randomized Trial. N Engl J Med 2020;382:503-13.
4. Sodickson A, Baeyens PF, Andriole KP, et al. Recurrent CT, cumulative radiation exposure, and associated radiation-induced cancer risks from CT of adults. Radiology 2009;251:175-84.
5. Marant-Micallef C, Shield KD, Vignat J, et al. The risk of cancer attributable to diagnostic medical radiation: Estimation for France in 2015. Int J Cancer 2019;144:2954-63.
6. Bergin CJ, Glover GM, Pauly J. Magnetic resonance imaging of lung parenchyma. J Thorac Imaging 1993;8:12-7.
7. Meier-Schroers M, Homsi R, Gieseke J, et al. Lung cancer screening with MRI: Evaluation of MRI for lung cancer screening by comparison of LDCT- and MRI-derived Lung-RADS categories in the first two screening rounds. Eur Radiol 2019;29:898-905.
8. Raptis CA, Ludwig DR, Hammer MM, et al. Building blocks for thoracic MRI: Challenges, sequences, and protocol design. J Magn Reson Imaging 2019;50:682-701.
9. Ohno Y, Kauczor HU, Hatabu H, et al. MRI for solitary pulmonary nodule and mass assessment: Current state of the art. J Magn Reson Imaging 2018;47:1437-58.
10. Lee CU, White DB, Sykes AM. Establishing a chest MRI practice and its clinical applications: our insight and protocols. J Clin Imaging Sci 2014;4:17.
11. Kumar S, Rai R, Stemmer A, et al. Feasibility of free breathing Lung MRI for Radiotherapy using non-Cartesian k-space acquisition schemes. Br J Radiol 2017;90:20170037.
12. Kida I, Ueguchi T, Matsuoka Y, et al. Comparison of Diffusion-Weighted Imaging in the Human Brain Using Readout-Segmented EPI and PROPELLER Turbo Spin Echo With Single-Shot EPI at 7 T MRI. Invest Radiol 2016;51:435-9.
13. Zhang L, Tian C, Wang P, et al. Comparative study of image quality between axial T2-weighted BLADE and turbo spin-echo MRI of the upper abdomen on 3.0 T. Jpn J Radiol 2015;33:585-90.
14. Cieszanowski A, Lisowska A, Dabrowska M, et al. MR Imaging of Pulmonary Nodules: Detection Rate and Accuracy of Size Estimation in Comparison to Computed Tomography. PLoS One 2016;11:e0156272.
15. Burris NS, Johnson KM, Larson PE, et al. Detection of Small Pulmonary Nodules with Ultrashort Echo Time Sequences in Oncology Patients by Using a PET/MR System. Radiology 2016;278:239-46.
16. MacMahon H, Naidich DP, Goo JM, et al. Guidelines

for Management of Incidental Pulmonary Nodules Detected on CT Images: From the Fleischner Society 2017. Radiology 2017;284:228-43.
17. American College of Radiology Committee on Lung-RADS®. Lung-RADS Assessment Categories version1.1. Available online: https://www.acr.org/-/media/ACR/Files/RADS/Lung-RADS/LungRADSAssessmentCategoriesv1-1.pdf. Accessed on August 7, 2021.
18. Bae K, Jeon KN, Hwang MJ, et al. Comparison of lung imaging using three-dimensional ultrashort echo time and zero echo time sequences: preliminary study. Eur Radiol 2019;29:2253-62.
19. Meier-Schroers M, Homsi R, Schild HH, et al. Lung cancer screening with MRI: characterization of nodules with different non-enhanced MRI sequences. Acta Radiol 2019;60:168-76.
20. de Galiza Barbosa F, Geismar JH, Delso G, et al. Pulmonary nodule detection in oncological patients - Value of respiratory-triggered, periodically rotated overlapping parallel T2-weighted imaging evaluated with PET/CT-MR. Eur J Radiol 2018;98:165-70.
21. Nagel SN, Wyschkon S, Schwartz S, et al. Can magnetic resonance imaging be an alternative to computed tomography in immunocompromised patients with suspected fungal infections? Feasibility of a speed optimized examination protocol at 3 Tesla. Eur J Radiol 2016;85:857-63.
22. Meier-Schroers M, Homsi R, Skowasch D, et al. Lung cancer screening with MRI: results of the first screening round. J Cancer Res Clin Oncol 2018;144:117-25.
23. Schwenzer NF, Seith F, Gatidis S, et al. Diagnosing Lung Nodules on Oncologic MR/PET Imaging: Comparison of Fast T1-Weighted Sequences and Influence of Image Acquisition in Inspiration and Expiration Breath-Hold. Korean J Radiol 2016;17:684-94.
24. Renz DM, Herrmann KH, Kraemer M, et al. Ultrashort echo time MRI of the lung in children and adolescents: comparison with non-enhanced computed tomography and standard post-contrast T1w MRI sequences. Eur Radiol 2022;32:1833-42.
25. Ohno Y, Koyama H, Yoshikawa T, et al. Standard-, Reduced-, and No-Dose Thin-Section Radiologic Examinations: Comparison of Capability for Nodule Detection and Nodule Type Assessment in Patients Suspected of Having Pulmonary Nodules. Radiology 2017;284:562-73.
26. Wielpütz MO, Lee HY, Koyama H, et al. Morphologic Characterization of Pulmonary Nodules With Ultrashort TE MRI at 3T. AJR Am J Roentgenol 2018;210:1216-25.
27. Yang S, Shan F, Yan Q, et al. A pilot study of native T1-mapping for focal pulmonary lesions in 3.0 T magnetic resonance imaging: size estimation and differential diagnosis. J Thorac Dis 2020;12:2517-28.
28. Henz Concatto N, Watte G, Marchiori E, et al. Magnetic resonance imaging of pulmonary nodules: accuracy in a granulomatous disease-endemic region. Eur Radiol 2016;26:2915-20.
29. Yang A, Xiao XH, Wang ZL, et al. Carotid wall imaging with 3D_T2_FFE: sequence parameter optimization and comparison with 3D_T2_SPACE. Sci Rep 2021;11:2255.
30. Dang S, Gao X, Ma G, et al. Combination of free-breathing radial 3D fat-suppressed T1-weighted gradient-echo sequence with diffusion weighted images: Potential for differentiating malignant from benign peripheral solid pulmonary masses. Magn Reson Imaging 2019;57:271-6.
31. Chandarana H, Block TK, Rosenkrantz AB, et al. Free-breathing radial 3D fat-suppressed T1-weighted gradient echo sequence: a viable alternative for contrast-enhanced liver imaging in patients unable to suspend respiration. Invest Radiol 2011;46:648-53.

Cite this article as: Yang S, Shan F, Shi Y, Liu T, Wang Q, Zhang H, Zhang X, Yang S, Zhang Z. Sensitivity and specificity of magnetic resonance imaging in routine diagnosis of pulmonary lesions: a comparison with computed tomography. J Thorac Dis 2022;14(10):3762-3772. doi: 10.21037/jtd-22-370

Supplementary

Table S1 The lesions' LMR in each sequence

	Low	Moderate	High
T1WI-VIBE	9	80	11
T1WI-starVIBE	11	89	0
T2WI-fBLADE	4	15	81
T2WI-SPACE	1	18	81

LMR, lesion to muscle ratio.

https://dx.doi.org/10.21037/jtd-22-370